

Iron-induced relaxation mechanisms in the human substantia nigra: towards quantifying iron load in dopaminergic neurons

Malte David Brammerloh^{1,2}, Isabel Weigelt³, Thomas Arendt³, Filippos Gavriilidis², Nico Scherf², Steffen Jankuhn⁴, Markus Morawski³, Nikolaus Weiskopf², and Evgeniya Kirilina²

¹Faculty of Physics and Earth Sciences, Leipzig University, Leipzig, Germany, ²Department of Neurophysics, Max Planck Institute for Human Cognitive and Brain Sciences, Leipzig, Germany, ³Paul Flechsig Institute of Brain Research, Leipzig, Germany, ⁴Felix Bloch Institute for Solid State Physics, Leipzig University, Leipzig, Germany

Synopsis

Pathological iron accumulation in the human brain is a biomarker for neurodegeneration. Several diagnostically promising MR-based methods for in vivo iron quantification were proposed, based on the empirical relationship between R_2^* and iron concentration. However, these do not account for different chemical forms and cellular distribution of iron. We combined post mortem MRI, advanced quantitative histology and biophysical modeling to develop a generative theory linking obtained iron concentrations to quantitative MR parameters. The impact of nanoscale molecular interaction of water with iron and of iron-rich dopaminergic neurons was quantified in substantia nigra.

Introduction

Pathologic iron accumulation is a biomarker and potential cause of several neurodegenerative diseases. In Parkinson's disease (PD) iron overload in dopaminergic neurons (DN) may lead to neuronal loss in substantia nigra (SN), especially in nigrosome 1 (N1).¹ Several diagnostically promising MR-based methods for in vivo iron quantification were proposed.^{2,3} These methods mostly utilize R_2 and QSM related contrasts and are based on the empirical relationship between iron concentration and MR parameters.^{4,5}

However, this is an oversimplification and the iron-induced MR-contrast in the human brain is poorly understood. The contribution of different chemical forms of iron and different types of iron-containing cells is unknown. Moreover, the role of relaxation mechanisms resulting from either nanoscale molecular interaction of water with iron or from microscopic local field perturbations induced by iron-rich cells has not been quantified yet. Understanding these different relaxation contributions is indispensable in order to develop diagnostic markers with high specificity.

We aim to close this gap by quantifying the contribution to relaxation of several mechanisms in SN. To this end, we combined post mortem MRI, advanced quantitative iron histology and biophysical modeling (Figure 1). We quantified the contribution of the two major chemical forms of iron: iron chelator neuromelanin inside and the storage protein ferritin outside the DN. We developed a generative theory linking histologically obtained cellular iron concentrations with quantitative R_2^* and R_2 maps and compared the theoretical predictions with the experiment.

Methods

Quantitative MRI measurements were performed on two post mortem human brain specimen containing SN at 7 T (Magnetom, Siemens, Erlangen). R_2^* was estimated from a 3D multi-echo FLASH (isotropic resolution of 0.23 mm, $TE_{1...7}=7...46$ ms, $TR=300$ ms), R_1 from a MP2RAGE (isotropic resolution 0.3 mm, $T_{1,2}=0.12,0.9$ s, $TR=3$ s) and R_2 from a spin echo sequence (0.24 mm, $TE_{1...5}=30...75$ ms).

Quantitative microscopic iron maps in 3D were obtained using ten adjacent 10 μ m sections stained with Perls' for iron, which were calibrated using quantitative iron maps obtained with Proton Induced X-ray Emission (PIXE). Iron quantification inside and outside the DN was possible using nickel-enhanced immunohistochemistry for neuron detection in the PIXE maps and image segmentation of Perls' stain using a classifier implemented in Fiji.⁶

Generative biophysical models describing the following relaxation mechanisms were developed using the obtained iron maps.

- The relaxation caused by molecular interaction of water protons with iron bound to ferritin and neuromelanin were estimated using solution relaxivities of both compounds.^{7,8}
- The impact of microscopic cellular distribution of iron to R_2^* relaxation rate was estimated in a two-step approach:
 1. The local field perturbation within MRI voxels and resulting MRI signal decays in static dephasing regime were calculated.
 2. The influence of water diffusion was included using Monte Carlo simulations and motional narrowing theory.⁹

Relaxation rate maps for each relaxation mechanisms were compared to experimental quantitative MRI maps.

Results

Quantitative 3D iron map of human SN showed inhomogeneous iron distributions at the macroscopic and microscopic scales (Figure 2). Neuromelanin iron was found in the nigrosomes, ferritin iron in the entire SN. N1 showed lower total iron level, but a more inhomogeneous iron distribution. Biophysical modeling of iron-induced MRI contrast demonstrated that the gradient echo signal in SN is a combination of mono- and quadratic exponential decays, with the monoexponential decay originating mostly, but not solely, from iron in DN (Figure 3). Estimated maps of the transverse relaxation rate induced by molecular interaction with neuromelanin (A) and ferritin (B) iron are shown in Figure 4. The upper limit for the iron-induced R_2' relaxation rate was derived in the static dephasing regime directly from the quantitative iron maps. According to theoretical estimations the inhomogeneous distribution of iron at the microscopic scale is a dominant relaxation mechanism in SN. However, a quantitative comparison of estimated R_2^* with experiments shows that theory strongly underestimates R_2^* . Among studied relaxation mechanisms molecular interaction with ferritin iron demonstrated the highest spatial correlation with experimental maps of R_2^* (Figure 4B,E).

Discussion and Conclusion

We have developed a biophysical model predicting the contributions of different chemical forms of iron and cellular distribution of iron to iron-induced relaxation in human SN. We showed the possibility to disentangle the contributions to R_2^* relaxation of NM and ferritin iron by a line shape analysis as a first step to DN quantification in vivo. We demonstrated that different relaxation mechanisms result in different patterns of R_2^* relaxation. Modeling the molecular interactions with ferritin iron showed the highest spatial correlation with measured relaxation rates, but underestimates it by an order of magnitude. This might point towards additional relaxation mechanisms absent in ferritin solutions. Our results provide an important step towards quantitative understanding of iron-induced relaxation mechanisms in human SN.

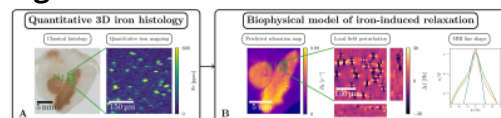
Acknowledgements

The research leading to these results has received funding from the European Research Council under the European Union's Seventh Framework Program (FP7/2007-2013) / ERC grant agreement n° 616905. This project has also received funding from the BMBF (01EW1711A & B) in the framework of ERA-NET NEURON.

References

1. F. A. Zucca, J. Segura-Aguilar, E. Ferrari, et al. Interactions of iron, dopamine and neuromelanin pathways in brain aging and Parkinson's disease. *Prog Neurobiol.* 2017;155:96–119.
2. M. F. Callaghan, P. Freund, B. Draganski, et al. Widespread age-related differences in the human brain microstructure revealed by quantitative magnetic resonance imaging. *Neurobiol. Aging.* 2014;35(8):1862–1872.
3. C. Langkammer, N. Krebs, W. Goessler, et al. Quantitative MR Imaging of Brain Iron: A Postmortem Validation Study. *Radiology.* 2010;257(2):455-462.
4. C. Langkammer, F. Schweser, N. Krebs, et al. Quantitative susceptibility mapping (QSM) as a means to measure brain iron? A post mortem validation study. *NeuroImage.* 2012;62(3):1593-1599.
5. C. Stüber, M. Morawski, A. Schäfer, et al. Myelin and iron concentration in the human brain: A quantitative study of MRI contrast. *NeuroImage.* 2014;93(1):95-106.
6. I. Arganda-Carreras, V. Kaynig, C. Rueden et al. Trainable Weka Segmentation: a machine learning tool for microscopy pixel classification. *Bioinformatics.* 2017;33(15):2424-2426.
7. Y. Gossuin, A. Roch, R. N. Muller, and P. Gillis. Relaxation induced by ferritin and ferritin-like magnetic particles: The role of proton exchange. *Magn Reson Med.* 200;43(2):237–243.
8. P. Trujillo, P. E. Summers, E. Ferrari, et al. Contrast mechanisms associated with neuromelanin-MRI. *Magn Reson Med.* 2017;78(5):1790–1800.
9. D. S. Novikov and V. G. Kiselev. Transverse NMR relaxation in magnetically heterogeneous media. *J Magn Reson.* 2008;195(1):33-39.

Figures



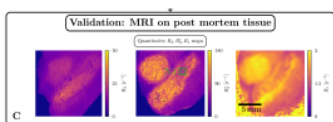


Figure 1: Methods overview. A: 3D quantitative maps of ferritin and neuromelanin iron in human SN were obtained by Perls' stain for on consecutive sections combined with quantitative iron mapping using PIXE. B: Biophysical models of iron-induced relaxation rates were developed based on these maps: Relaxation rates induced by molecular interactions of ferritin and neuromelanin iron with water were estimated using known relaxivities of both processes in solution. Relaxation rates induced by cellular iron distribution were obtained by analysis of field perturbations by iron-rich cells. C: Theoretical predictions for relaxation mechanisms were compared to quantitative experimental MR parameters of the same specimen.

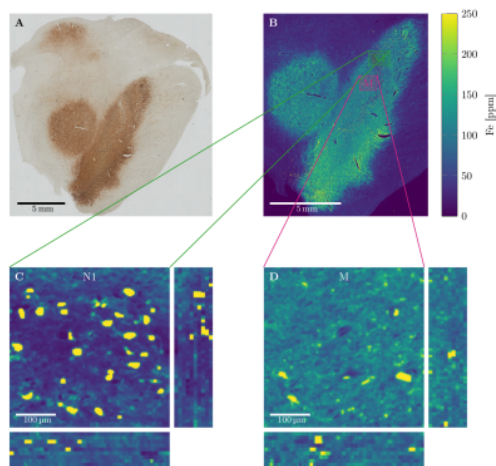


Figure 2: 3D quantitative iron maps. A: Histological Perls' stains for ferric iron were transformed using Lambert-Beer law and calibrated with PIXE in order to obtain 3D quantitative iron maps (B). Dopaminergic neurons were segmented in Perls' images using Trainable Weka Segmentation in Fiji. Two regions of interest were used for in detail analysis: one region in nigrosome 1 (N1) (C) and one in the nigral matrix (M) (D). The concentration scale for B,C and D is shown next to B.

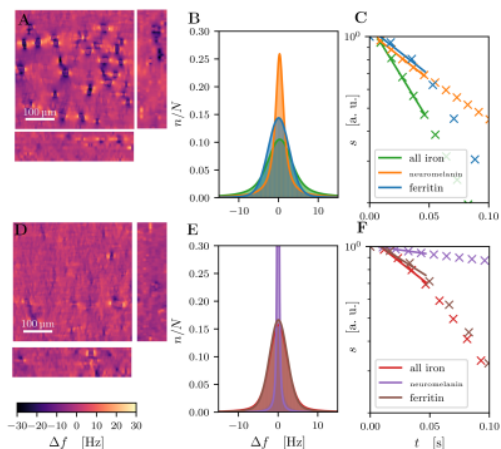
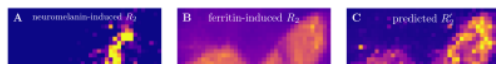


Figure 3: Analysis of static dephasing in nigrosome 1 (N1) (A,B,C) and nigral matrix (M) (D,E,F) (cf. Figure 2 for N1 and M locations). A,D: 3D Larmor frequency perturbation maps. B,E: Intravoxel frequency distributions induced by entire iron, neuromelanin inside and ferritin outside of dopaminergic neurons. Voigt profiles fits to the histograms are shown as lines. This profile is a convolution of a Lorentzian and a Gaussian, corresponding to the mono- and quadratic exponential signal decay. C,F: R_2' decays obtained from the frequency distributions by Fourier transform. Neuromelanin-bound iron contributes a monoexponential decay, whereas ferritin-bound iron contributes a mostly quadratic exponential decay.



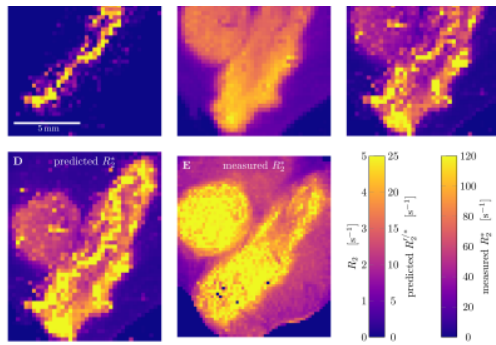


Figure 4: Theoretical prediction of several relaxation mechanisms compared with experiment. Predicted R_2 rate induced by molecular interactions with neuromelanin (A) and ferritin (B). C: Predicted dephasing rate R_2' induced by cellular iron distribution. D: Total predicted iron-induced R_2^* , the sum of contributions from A, B and C. E: Experimentally measured R_2^* . The dephasing is predicted to be the dominant contribution to relaxation. The ferritin induced contribution R_2 shows the highest spatial correlation to the experiment. The theoretical predictions underestimate R_2^* indicating additional relaxation mechanisms.